Check for updates

Fully metallic frequency selective surface (FSS) circular polarizer based on cost-effective chemical etching manufacturing technique

Wai Yan Yong,[1,2,✉] Arjen Velkers,[1] and Andrés Alayón Glazunov[1,3]

[1] *Department of Electrical Engineering, University of Twente, Enschede, Netherlands*

[2] *Rohde & Schwarz GmbH & Co.KG, Munich, Germany*

[3] *Department of Science and Technology, Linköping University, Norrköping, Sweden*

✉ Email: w.y.yongwaiyan@utwente.nl

This letter presents a fully metallic circular polarizer based on a bandpass frequency selective surface (FSS) that converts linear polarization (LP) to circular polarization (CP) in the Ka-band. The proposed FSS circular polarizer consists of three cascaded identical perforated metal screens. The Jerusalem slot is used as the element of the FSS circular polarizer to produce an entirely metallic screen with a compact footprint. The Jerusalem slot allows the all-metallic design to be realized without mechanical issues. A 35 × 35 elements prototype has been designed and manufactured using a cost-effective chemical metallic etching technique, and performed measurements agree well with the numerical simulations. At broadside direction ($\theta = 0°$), the proposed polarizer operates from 27.5–30.1 GHz, while at the oblique angle of incidence $\theta = 20°$, the operating frequency is reduced to 27.7–29.4 GHz. The manufactured prototype has a low insertion loss (IL), i.e. $IL_{max} \leq 1$ dB and a good axial ratio performance, i.e. AR ≤ 2 dB at the desired operating frequency band. Thus, based on a cost-effective manufacturing technique, the proposed circular polarizer demonstrates an excellent approach to devising all-metallic FSS polarizers with good IL.

Introduction: Circular polarization (CP) waves may offer numerous advantages as compared to the linear polarization (LP) waves, e.g. reduced polarization mismatch, low susceptibility to multipath, reduced rain echo, absorption, and reflection effects [1, 2]. Conventionally, CP waves can be mainly generated by two techniques: the direct generation of CP waves utilizing a CP antenna [3, 4], or the transformation of LP waves into CP waves using a polarizer [2, 5–8]. In the former method, an antenna consisting of a CP radiating element is designed, e.g. as the helical antenna [4], the log spiral antenna [3] and modified patch antenna or the dipole antenna [1, 9]. Alternately, the CP antenna can be realized by adding the appropriate phase shift to an LP antenna array [10]. On the other hand, the CP waves can be produced by combining an LP antenna with circular polarizers [2, 8, 11–14]. These circular polarizers can be designed using either FSS [12, 15] or metasurfaces [13]. Polarizers offer more design flexibility as they can be designed independently of the antenna and later cascaded with the antennas, which makes the design process considerably more robust [11, 12]. Recently, there has been a growing interest in developing all-metallic FSS circular polarizers [12, 16, 17] because undesired dielectric losses are absent. However, several challenges, such as the mechanical robustness consideration and miniaturization of the unit cell, must still be overcome before the design of an all-metallic FSS circular polarizer is feasible. Firstly, the mechanical considerations of the fully metallic FSS require connected elements, contrary to substrate-based systems, limiting design flexibility. Design freedom has recently been improved by introducing 3D printing technology, demonstrating behavioural agreement between designed and measured performance. Nevertheless, its application to entirely metallic constructions is still not competitive in terms of dimensional tolerance and surface roughness [16, 18]. Second, because permittivity-driven miniaturization is not feasible for all-metallic FSS structures, miniaturization of the unit cell periodicity is challenging [12]. Limited research has been conducted on all-metallic FSS polarizers in general and, more specifically, based on cost-effective manufacturing techniques [12, 16, 17].

Therefore, based on our investigation in this paper, we propose a low-cost all-metallic FSS circular polarizer for mmWave applications. The design comprises three identical perforated metallic screens separated by an air gap. Each aperture in the perforated metal screen comprises a periodically arranged array of JSs. The suggested JS-based geometry permits an all-metallic implementation with robust mechanical characteristics that is straightforward to manufacture while can be easily designed to obtain the circular polarization as two orthogonal slots are available to create the required 90° phase shift for the circular polarization generation. In addition, the proposed three-layer JS FSS structure exhibits a low insertion loss (IL) from 26.7–30.5 GHz. The proposed polarizer converts LP waves to CP waves at broadside direction ($\theta = 0°$) and at oblique angles of incidence up to ($\theta = 20°$) while satisfying the 3 dB axial ratio (AR) criterion. A prototype of the circular polarizer was manufactured using cost-effective chemical metallic etching. To the authors' best knowledge, it is the first time an all-metallic FSS circular polarizer has been manufactured using chemical metallic etching.

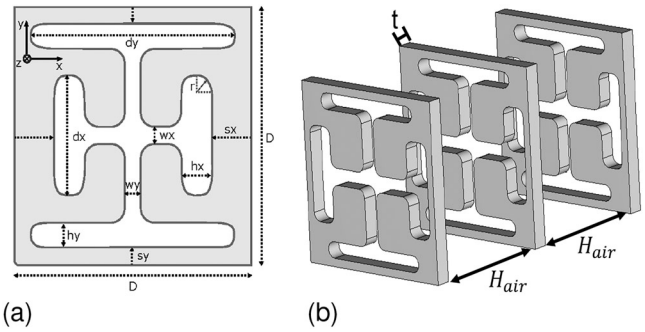

Fig. 1 *An artist representation of the proposed tri-layer JS circular polarizer, (a) unit cell top view and (b) tri-layer perspective view. The optimized parameters are given as $D = 3.3$ mm, $H_{air} = 2.5$ mm, $d_x = 1.7$ mm, $d_y = 2.3$ mm, $w_x = w_y = 0.3$ mm, $h_x = 0.5$ mm, $h_y = 0.3$ mm, and $s_x = s_y = 1.7$ mm, respectively*

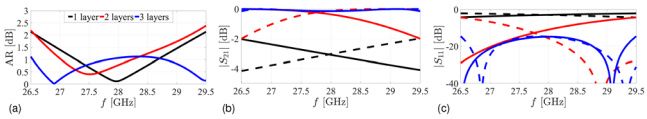

Fig. 2 *Simulated results of the proposed JS FSS circular polarizer with different metallic FSS layer operating at broadside direction ($\theta = 0°$) with (a) axial ratio* AR*, (b) transmission coefficient $|S_{21}|$, and (c) reflection coefficient $|S_{11}|$. The solid and dashed lines denote the* x- *and* y*-polarizations, respectively*

Design of the jerusalem slot FSS circular polarizer: The proposed JS FSS illustrated in Figure 1 is modelled and simulated using the CST Microwave Studio. The unit cell boundary condition was employed with the infinite array approximation excited by an ideal plane wave.

In Figure 1, the grey area represents the metal, and the white colour represents the etched slots. As can be seen, the horizontal (*y*-polarized) and vertical (*x*-polarized) slots of the proposed JS are asymmetric relative to each other. The dimensions of the JS's vertical and horizontal slots will predominantly influence the transmission performance (amplitude and phase) of the *y*-polarized and the *x*-polarized waves, respectively. These asymmetrical orthogonal slots with different dimensions operating in the same frequency range introduce a phase shift between the two polarizations. By adequately tuning these slots, the CP waves can be produced within the desired operating frequency band by introducing the required phased shift. The proposed FSS uses a 0.1 mm thick brass metallic screen in the initial design. Figure 2 shows the simulated performance of the proposed JS FSS circular polarizer with a different number of layers operating at broadside direction. Considering the AR ≤ 1.5 dB, the single layer FSS operates within the frequency range of 27.9–29 GHz. However, by increasing the number of FSS layers to three, the operating frequency range is enhanced to 26.5–29.5 GHz. The insertion loss performance exhibits a similar improvement. Indeed, for one layer, the IL_{max} is approximately 4 dB and improves to 0.3 dB when the number of JS FSS layers is increased to three. Both of these significant improvements in the AR and IL_{max} are the result of the improved impedance matching reflected by the S_{11} of both *x*- and *y*-polarized JS within the operating frequency band. Consequently, the remainder of the discussion will focus on the performance evaluation of the three-layer JS FSS circular polarizer.

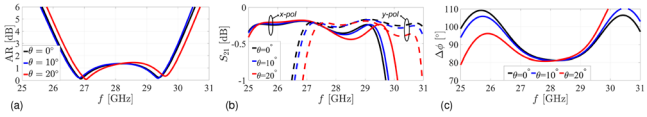

Fig. 3 *Simulated results of the proposed tri-layer JS FSS circular polarizer at both broadside and oblique angle of incidence, (a)* AR*, (b)* $|S_{21}|$*, and (c) different in the phase of the transmission coefficient between* x- *and* y*-polarization* $\Delta\phi$

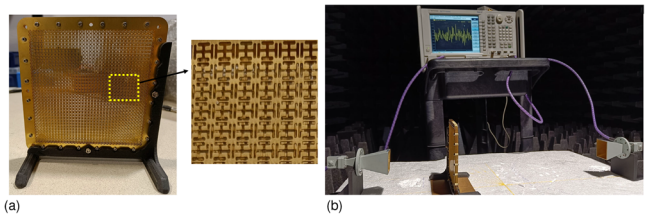

Fig. 4 *(a) Fabricated prototype of the proposed JS FSS circular polarizer and (b) the measurement setup*

The geometric dimensions of the proposed JS FSS circular polarizer are optimized using a parametric study. As depicted in Figure 1, all parameters are tuned and optimized to cover as much bandwidth as feasible within the 26.5–29.5 GHz band while maintaining an AR of less than 3 dB. Figure 3 shows the simulated results of the proposed JS FSS circular polarizer. As can be seen, the suggested JS FSS circular polarizer operates with AR $\leq$ 3 dB over 26–30 GHz in broadside direction ($\theta = 0^\circ$). In addition, the proposed polarizer demonstrates minimal IL performance, with $IL_{max} \leq 1$ dB over the operating frequency. However, as the scanned angle is increased to $\theta = 20^\circ$, the operating frequency of the proposed circular polarizer is shifted to high frequency. At $\theta = 20^\circ$, the proposed JS FSS circular polarizer could operate only at 26–29.8 GHz with an AR $\leq$ 3 dB. The deviation is due to the changing impedance of the JS FSS circular polarizer at an oblique incidence angle [19].

Experimental results and discussion: To experimentally validate the proposed JS FSS circular polarizer, a prototype consisting of a finite array with 35 × 35 elements was fabricated using the aforementioned cost-effective chemical metallic etching technique as shown in Figure 4. The Brass CuZn37 was used as the manufacturing material. Since the final prototype consists of 3 identical metallic screens (layers), several spacers with a height of approximately 2.5 mm are placed between the metallic screens for mechanical stability.

To evaluate the efficacy of the manufactured circular polarizer, the bi-static measurement setup depicted in Figure 4b was used. The distance between the transmitting antenna and the proposed polarizer must first be determined to satisfy the plane wave requirement as closely as possible. The conventional approach is to position the polarizer in the far field of the transmitting antenna [15, 20, 21]. However, this will necessitate the fabrication of an unpractically large circular polarizer to avoid undesirable edge effects. Positioning the proposed polarizer close to the transmitting antenna can minimize this edge effect for the circular polarizer of finite size, as in this study. The second scenario, in which the polarizer is positioned near the transmitting antenna, is also preferable in the practical deployment because it will reduce the antenna system's overall profile [14, 22, 23]. However, when the proposed circular polarizer is placed near the transmitting antenna, the waves impinging on the circular polarizer will become less planar. An alternative method for assessing the efficacy of the FSS is to place the designed FSS between two open-ended waveguides. However, this technique can solely be evaluated for the broadside direction [24]. Given the absence of a generally standardized guideline for determining the array size of the FSS and the measurement setup, one potential strategy involves identifying the distance between the transmit antenna and the polarizer that best satisfies the trade-off between the two scenarios. We initially evaluated the performance of the manufactured JS FSS circular polarizer for the broadside direction at various distances. The final location of the JS FSS circular polarizer was chosen to be placed 14 cm from the transmitting horn aperture. Figure 5 shows the measurement results of the proposed JS FSS circular polarizer. It is worth noting that time gating was applied in our measurement result to mitigate the unwanted reflections due to

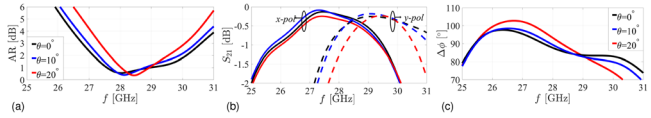

Fig. 5 *Measured results of the proposed JS FSS circular polarizer at both broadside and oblique angle of incidence, (a) the axial ratio (AR), (b) magnitude of the transmission coefficient, and (c) the phase difference of the transmission coefficient between* x- *and* y*-polarizations*

the measurement setup [25]. Also worth noticing is that the time gating will not mitigate the reflection caused by the polarizer [25].

Figure 5 shows the measured axial ratio AR of the manufactured JS FSS circular polarizer. As can be seen from the figure, at the broadside direction $\theta = 0^\circ$, the proposed JS FSS circular polarizer satisfies the AR $\leq$ 2 dB condition from 27.2–30.1 GHz. Compared to the simulation, the operating frequency of the manufactured prototype has been shifted by approximately 3%. This difference in the operating frequency is mainly due to unavoidable manufacturing errors. For oblique angles of incidence, the operating bandwidth is substantially narrower than the simulation result. As an example, at the oblique angle $\theta = 20^\circ$, the fabricated FSS operates within the frequency range of 27.6–29.4 GHz, with an AR $\leq$ 2 dB. This discrepancy between the measured and simulated results is mainly attributed to the edge effects of the polarizer. Compared to the unit cell simulation in the CST, which has an unlimited large periodic array, the edge effects considerably impact the manufactured finite array FSS prototype. As previously mentioned, the distance between the horn antenna and the FSS prototype has been modified in the proposed setup to replicate the impingement of a plane wave on the FSS prototype, as observed in the simulation. However, the effective area of the FSS identified by the horn antenna is substantially smaller at oblique angles. One technique is to build a very large polarizer, which is impractical for most practical deployments. Another approach is co-simulating the antenna and the polarizer [13, 14]. This approach, however, is computationally intensive and is currently confined to broadside direction evaluation [13, 14]. To deal with this issue, our future research efforts will prioritize the fabrication of the FSS with varying array sizes to conduct empirical investigations on the optimal array size for the finite FSS. It is worth noting that the proposed JS FSS orthogonal slots are designed with different dimensions but operate at the same frequency to provide the phase shift required for circular polarization transformation. Consequently, it is necessary to characterize the transmission coefficient $|S_{21}|$ of the JS FSS for both *x*- and *y*-polarization and their magnitude and phase. Figures 5b and 5c show the magnitude and phase of the measurement of the S_{21} for both *x*- and *y*-polarized slots, respectively. As can be seen, the insertion loss IL ranges from 0.2–1 dB over its operating frequency for both *x*- and *y*-polarized slots. It is worth noting that the measured IL_{max} is slightly higher than the simulated results due to the additional surface roughness in the prototype. On the other hand, the phase difference of the orthogonal JS over the operating frequency with AR $\leq$ 2 dB is approximately $90 \pm 10^\circ$.

Table 1 compares the proposed JS FSS circular polarizer and the existing published all-metallic FSS circular polarizer. To the authors' knowledge, it is the first time that an all-metallic FSS circular polarizer has been fabricated using the chemical metallic etching technique. As compared to the slot-type FSS presented in [12], our solution using the JS FSS allowed us to produce a much more compact design with AR $\leq$ 1 dB at an oblique angle of incidence up to $\theta = 20^\circ$. Nevertheless, as mentioned above, the operation at oblique angles comes with bandwidth reduction.

Conclusion: This letter proposed a fully metallic circular polarizer based on the JS bandpass FSS. The proposed polarizer comprises three cascaded metallic screens (layers) with perforations. Thanks to the JS, the unit cell dimension of the FSS circular polarizer has been substantially reduced compared to similar published designs. Good performance was obtained at both broadside ($\theta = 0^\circ$) and oblique angles of incidence up to $\theta = 20^\circ$. However, at oblique angles of incidence, the operating frequency is reduced by 6%, which can be explained by the change in impedance resulting in a phase imbalance between the two orthogonal JSs. In addition, it is proposed for the first time to manufacture the all-metallic circular polarizer using the cost-effective chemical

13509911x, 2023, 20, Downloaded from https://ietresearch.onlinelibrary.wiley.com/doi/10.1049/ell2.12982 by University Of Twente Finance Department, Wiley Online Library on [21/05/2024]. See the Terms and Conditions (https://onlinelibrary.wiley.com/terms-and-conditions) on Wiley Online Library for rules of use; OA articles are governed by the applicable Creative Commons License

Table 1. Performance comparison of existing fully metallic FSS circular polarizers. f is the operating frequency, BW is the bandwidth, and IL_{max} is the higher insertion loss of the proposed FSS from either x- *or* y*-polarization*

Ref.	f [GHz]	Unit Cell Periodicity	IL_{max} [dB]	AR $\leq$ 2 dB [%]	Angular Stability	Fabrication Technology
[12]	19.7–20.2/29.5–30	$0.96\lambda_h$	≤ 0.7	$\approx 2.5/1.7$	Broadside only	Milling (Water cutting)
[16]	19–29	$0.52\lambda_h$	1–1.5	≤ 37.8	up to 30°	3D printing
[17]	9.7–10.3/14.6–15.6	$\leq 0.5\lambda_h$	≥ 3.2	$\leq 5.8/2.3$	up to 20°	3D printing
[26]	3.24–3.99	N/A	≤ 1.65	≤ 21.9	up to 40°	Milling (Water cutting)
This work	27.5–30.1 (broadside)	$0.33\lambda_h$	≤ 0.5	≤ 11.1	up to 20°	Chemical etching
This work	27.7–29.5 (at $\theta = 20°$)		≤ 1	≤ 7.01	with reduction of band width	

metallic etching method. The proposed polarizer manufactured with the cost-effective chemical etching process has comparable performance to metallic FSS manufactured with conventional methods such as milling and 3D printing. Our future study will concentrate on establishing the appropriate array size of the finite FSS close to the simulation in the infinite array FSS.

Author contributions: Wai Yan Yong: Conceptualization, formal analysis, investigation, methodology, supervision, writing - original draft, writing - review and editing. Arjen Velkers: Conceptualization, validation. Andrés Alayón Glazunov: Supervision, writing - review and editing.

Acknowledgments: The authors would like to thank Gapwaves AB for fabricating the prototype. This work has received funding from the European Union's Horizon 2020 research and innovation program under the Marie Sklodowska-Curie grant agreement No. 766231 – WAVECOMBE – H2020-MSCA-ITN-2017. Funding from the ELLIIT strategic research environment (https://elliit.se/) is also appreciated. Wai Yan Yong was with the University of Twente when this research was conducted.

Conflict of interest: The authors declare no conflict of interest.

Data availability statement: Data available on request from the authors.

© 2023 The Authors. *Electronics Letters* published by John Wiley & Sons Ltd on behalf of The Institution of Engineering and Technology.

This is an open access article under the terms of the Creative Commons Attribution-NonCommercial License, which permits use, distribution and reproduction in any medium, provided the original work is properly cited and is not used for commercial purposes.

Received: *21 August 2023* Accepted: *4 October 2023*
doi: 10.1049/ell2.12982

References

1 Low, K.K.W., et al.: A 17.7–20.2-GHz 1024-element K-band SATCOM phased-array receiver with 8.1-dB/KG/T,±70° beam scanning, and high transmit isolation. *IEEE Trans. Microwave Theory Tech*. **70**(3), 1769–1778 (2022)
2 Chang, X., et al.: Shared-aperture phased array antenna with codesigned near-field coupled circular polarizer loaded for K/Ka-band wide-angle satellite communication. *IEEE Trans. Antennas Propag*. **70**(9), 7478–7490 (2022)
3 Zhang, T.L., et al.: Millimeter-wave ultrawideband circularly polarized planar array antenna using bold-C spiral elements with concept of tightly coupled array. *IEEE Trans. Antennas Propag*. **69**(4), 2013–2022 (2020)
4 Junkin, G.: A circularly polarized single-frequency multimode helical beam antenna. *IEEE Trans. Antennas Propag.* **67**(3), 1459–1466 (2018)
5 Morrow, I., Thomas, P.: Compact frequency selective surface for polarisation transform. *Electron. Lett.* **50**(2), 64–65 (2014)
6 Low, K.K.W., et al.: A 27–31-GHz 1024-element Ka-band SATCOM phased-array transmitter with 49.5-dBW peak EIRP, 1-dB AR, and ±70 beam scanning. *IEEE Trans. Microwave Theory Tech*. **70**(3), 1757–1768 (2022)
7 Sofi, M.A., Saurav, K., Koul, S.K.: Frequency-selective surface-based compact single substrate layer dual-band transmission-type linear-to-circular polarization converter. *IEEE Trans. Microwave Theory Tech.* **68**(10), 4138–4149 (2020)
8 Ma, Z.L., et al.: 3-D printed annular linear-to-circular dielectric polarizer and its applications to omnidirectional and multibeam antennas. *IEEE Trans. Antennas Propag*. **70**(10), 9365–9375 (2022)
9 Kazan, O., et al.: An 8-channel 5–33-GHz transmit phased array beamforming IC with 10.8–14.7-dBm PSAT for *C*-, *X*-, *Ku*-, and *Ka*-band SATCOM. *IEEE Trans. Microwave Theory Tech*. **71**(5), 2029–2039 (2023)
10 Lu, C., et al.: A millimeter-wave tunable hybrid-transformer-based circular polarization duplexer with sequentially-rotated antennas. *IEEE Trans. Microwave Theory Tech*. **64**(1), 166–177 (2015)
11 Akbari, M., et al.: Ka-band linear to circular polarization converter based on multilayer slab with broadband performance. *IEEE Access* **5**, 17927–17937 (2017)
12 Lundgren, J., et al.: Fully metallic dual-band linear-to-circular polarizer for K/K a-band. *IEEE Antennas Wireless Propag. Lett*. **20**(11), 2191–2195 (2021)
13 Lin, Q.W., et al.: A wideband circularly polarized antenna based on anisotropic metamaterial. *IEEE Trans. Antennas Propag*. **71**(2), 1254–1262 (2023)
14 Yin, J.Y., et al.: A circular polarizer with beamforming feature based on frequency selective surfaces. *Sci. Rep*. **7**(1), 41505 (2017)
15 Li, H., Li, B., Zhu, L.: Direct synthesis and design of wideband linear-to-circular polarizers on 3-D frequency selective structures. *IEEE Trans. Antennas Propag.* **70**(10), 9385–9395 (2022)
16 Molero, C., et al.: Broadband 3D-printed polarizer based on metallic transverse electro-magnetic unit-cells. *IEEE Trans. Antennas Propag*. **70**(6), 4632–4644 (2022)
17 Jimenez, C.M., Menargues, E., García-Vigueras, M.: All-metal 3-D frequency-selective surface with versatile dual-band polarization conversion. *IEEE Trans. Antennas Propag.* **68**(7), 5431–5441 (2020)
18 Zhang, B., et al.: Investigation on 3-D-printing technologies for millimeter-wave and terahertz applications. *Proc. IEEE* **105**(4), 723–736 (2017)
19 Munk, B.A.: *Frequency Selective Surfaces: Theory and Sesign*. Wiley, New York (2005)
20 Zhang, W., Li, J.Y., Xie, J.: A broadband circular polarizer based on cross-shaped composite frequency selective surfaces. *IEEE Trans. Antennas Propag.* **65**(10), 5623–5627 (2017)
21 Mirza, H., et al.: Deployable linear-to-circular polarizer using PDMS based on unloaded and loaded circular FSS arrays for Pico-Satellites. *IEEE Access* **7**, 2034–2041 (2018)
22 Li, L., et al.: Novel polarization-reconfigurable converter based on multilayer frequency-selective surfaces. *Proc. IEEE* **103**(7), 1057–1070 (2015)
23 Arnieri, E., et al.: A SIW-based polarization rotator with an application to linear-to-circular dual-band polarizers at K-/Ka-band. *IEEE Trans. Antennas Propag*. **68**(5), 3730–3738 (2020)
24 Sarabandi, K., Behdad, N.: A frequency selective surface with miniaturized elements. *IEEE Trans. Antennas Propag.* **55**(5), 1239–1245 (2007)
25 Hosseini, M., Hum, S.V.: A semianalytical approach to designing high-transparency low-profile circular polarizers. *IEEE Trans. Antennas Propag.* **66**(12), 7138–7147 (2018)
26 Dicandia, F.A., Genovesi, S.: Linear-to-circular polarization transmission converter exploiting meandered metallic slots. *IEEE Antennas Wireless Propag. Lett.* **21**(11), 2191–2195 (2022)

1350911x, 2023, 20, Downloaded from https://ietresearch.onlinelibrary.wiley.com/doi/10.1049/ell2.12982 by University Of Twente Finance Department, Wiley Online Library on [21/05/2024]. See the Terms and Conditions (https://onlinelibrary.wiley.com/terms-and-conditions) on Wiley Online Library for rules of use; OA articles are governed by the applicable Creative Commons License